Journal of Hazardous Materials 192 (2011) 1210–1218

Contents lists available at ScienceDirect

Journal of Hazardous Materials

journal homepage: www.elsevier.com/locate/jhazmat

Adsorption characteristics of haloacetonitriles on functionalized silica-based porous materials in aqueous solution

Panida Prarat[a,b], Chawalit Ngamcharussrivichai[c,d], Sutha Khaodhiar[e], Patiparn Punyapalakul[b,e,*]

[a] International Postgraduate Programs in Environmental Management, Graduate School, Chulalongkorn University, Bangkok 10330, Thailand
[b] Center of Excellence for Environmental and Hazardous Waste Management (EHWM), Chulalongkorn University, Bangkok 10330, Thailand
[c] Department of Chemical Technology, Faculty of Science, Chulalongkorn University, Bangkok 10330, Thailand
[d] Center for Petroleum, Petrochemicals and Advanced Materials, Chulalongkorn University, Bangkok 10330, Thailand
[e] Department of Environmental Engineering, Faculty of Engineering, Chulalongkorn University, Bangkok 10330, Thailand

ARTICLE INFO

Article history:
Received 28 March 2011
Received in revised form 13 June 2011
Accepted 13 June 2011
Available online 12 July 2011

Keywords:
Adsorption
Haloacetonitrile
Hexagonal mesoporous silicate
Surface functional group

ABSTRACT

The effect of the surface functional group on the removal and mechanism of dichloroacetonitrile (DCAN) adsorption over silica-based porous materials was evaluated in comparison with powdered activated carbon (PAC). Hexagonal mesoporous silicate (HMS) was synthesized and functionalized by three different types of organosilanes (3-aminopropyltriethoxysilane, 3-mercaptopropyltrimethoxysilane and *n*-octyldimethysilane). Adsorption kinetics and isotherm models were used to determine the adsorption mechanism. The selective adsorption of five haloacetonitriles (HANs) in the single and mixed solute systems was also studied. The experiments revealed that the surface functional groups of the adsorbents largely affected the DCAN adsorption capacities. 3-Mercaptopropyl-grafted HMS had a high DCAN adsorption capacity compared to PAC. The adsorption mechanism is believed to occur via an ion–dipole electrostatic interaction in which water interference is inevitable at low concentrations of DCAN. In addition, the adsorption of DCAN strongly depended on the pH of the solution as this related to the charge density of the adsorbents. The selective adsorption of the five HANs over PAC was not observed, while the molecular structure of different HANs obviously influenced the adsorption capacity and selectivity over 3-mercaptopropyl-grafted HMS.

© 2011 Elsevier B.V. All rights reserved.

1. Introduction

Haloacetonitriles (HANs) can be formed as by-products from the reaction between chlorine, chloramine or bromine disinfectants and natural organic matter present in drinking water supplies. Major HANs generated during the disinfection process consist of dichloroacetonitrile (DCAN), bromochloroacetonitrile (BCAN), dibromoacetonitrile (DBAN) and trichloroacetonitrile (TCAN). Due to their potential health effects, the World Health Organization has suggested guideline values of 20 $\mu g\,L^{-1}$ for DCAN, 70 $\mu g\,L^{-1}$ for DBAN and 1 $\mu g\,L^{-1}$ for TCAN. Moreover, HANs have been included in the US Environmental Protection Agency Information Collection Rules and they may be considered in future US EPA regulations.

Various processes, such as adsorption [1–4], ozonation [2] and membrane filtration [5], have been employed to remove the disinfection by-products (DBPs). Adsorption technology has been favored due to its advantages of low cost and simplicity. Activated carbon is predominantly used as the adsorbent because of its availability and high efficiency for the removal of a number of DBPs. However, the use of activated carbon is sometimes problematic due to its low adsorption-selective nature and difficulty in its regeneration.

Among the porous materials, mesoporous silicates offer a number of potential advantages as adsorbents due to their high surface area, large pore volume and narrow pore size distribution. Moreover, their surface modification with various organosilanes, is very helpful in improving the adsorptive capacity and selectivity as a result of specific interactions. A limited amount of work on the adsorption of DBPs over mesoporous silicates has been reported previously. Hexagonal mesoporous silicates (HMSs) with different functionalized surfaces were shown to be effective adsorbents for the removal of dichloroacetic acid (DCAA) [6]. Moreover, the crystalline structure, surface area and surface functional groups, play crucial roles in the adsorption of DCAA at low concentrations [7].

To the best of our knowledge, the adsorption of HANs by HMS in aqueous solution has not been studied. For a better understanding of the adsorption mechanism, however, a comparative study is still needed to evaluate the impact of the molecular structure of DBPs on the adsorption behavior of the synthesized adsorbents. Thus, the purpose of this study emphasized the investigation of the effect of surface functional groups on the HANs' adsorption

* Corresponding author. Tel.: +66 2 218 6686; fax: +66 2 218 6666.
E-mail addresses: patiparn.p@eng.chula.ac.th, p_patiparn@yahoo.com (P. Punyapalakul).

0304-3894/$ – see front matter © 2011 Elsevier B.V. All rights reserved.
doi:10.1016/j.jhazmat.2011.06.032

Table 1
Physicochemical characteristics of PAC, HMS and the three functionalized HMS derivatives.

Adsorbents	Surface functional group	Surface characteristic	Pore size as diameter (nm)	BET surface area ($m^2\ g^{-1}$)	pH_{PZC}	Contact angle (θ)	Density of functional group ($\mu mol\ m^{-2}$)
HMS	Silanol	Hydrophilic	2.60[a]	712[a]	4.5–5.5[a]	45.06	–
A-HMS	Amino and silanol	Hydrophilic	3.95[a]	262[a]	9.5[a]	40.18	9.037
M-HMS	Mercapto and silanol	Hydrophobic	2.48[a]	912[a]	6.2[a]	89.65	2.554
OD-HMS	Octyl and silanol	Hydrophobic	2.36[b]	477[b]	4.0[b]	89.83	–
PAC	Carboxyl, phenyl and oxygen-containing groups	Hydrophobic	1.90[a]	980[a]	9.5[a]	58.34	–

[a] Ref. [7].
[b] Ref. [10].

efficiency and mechanism. DCAN was selected as a model HAN for batch adsorption experiments. The modification of HMS with three organic functional groups (3-aminopropyltriethoxysilane, 3-mercaptopropyltrimethoxysilane and *n*-octyldimethysilane) was employed to investigate the effect of surface functional groups on DCAN adsorption capacity. The equilibrium data were fitted with adsorption isotherm models, and the kinetic parameters were calculated to determine the likely adsorption mechanism. In addition, the effect of the solution pH and the selective adsorption of five different HAN compounds differing in halogen groups or numbers were investigated as single and mixed solutes.

2. Materials and methods

2.1. HMS and organic functionalized HMS syntheses

Synthesis of HMS followed the procedure described by Lee et al. [8]. Modified HMSs with 3-aminopropyltriethoxy-(A-HMS) and 3-mercaptopropyltrimethoxy-(M-HMS) were prepared via a co-condensation method following the procedure previously published [7,8]. *N*-octyldimethy-(OD-HMS) was prepared by a post-synthesis method as described by Inumura et al. [9].

2.2. Characterization of adsorbents

The physicochemical properties and XRD patterns of synthesized adsorbents have already been reported [7,10], but are summarized in Table 1 and Fig. 1, respectively for convenience of reference. The quantification of organosilanes grafted on HMS was performed by elemental analysis. An autoclave digestion in the presence of potassium persulfate in an alkaline media was conducted for determining the nitrogen content of A-HMS [11].

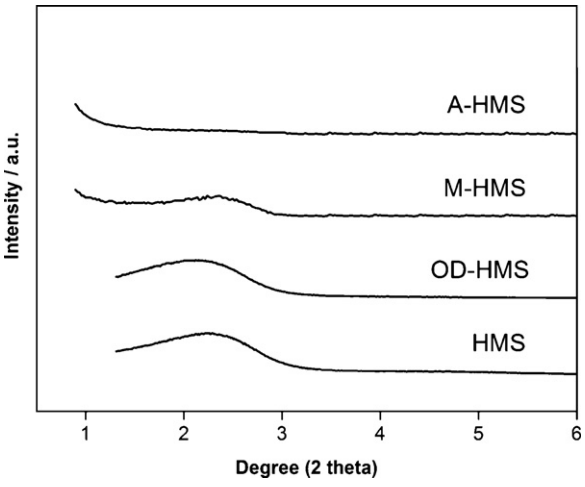

Fig. 1. Representative XRD patterns of HMS and the three functionalized HMS derivatives.

The amount of sulfur in M-HMS was measured by using a LECO SC132 sulfur analyzer. Hydrophobic/hydrophilic characteristics of the adsorbent surface were evaluated by measuring the water contact angle (θ) using a Dataphysics DCAT-11 tensiometer in a powder contact angle mode.

2.3. Adsorption study

The evaluation of the aqueous-phase adsorption of HANs was conducted as a batch experiment. In a typical procedure, 0.025 g of adsorbent and 35 mL of the respective HAN solution were mixed in a 100-mL Erlenmeyer flask covered with a glass stopper. The flask was then stirred in a rotary shaker at 25 °C, and then separated through a GF/C glass microfiber filter to remove the solids. The supernatant solution was analyzed by gas chromatography equipped with electron capture detector (GC/ECD) according to EPA method 551.1 [12]. Each experiment was performed in triplicate under identical conditions.

Kinetic studies were performed in 10 mM phosphate buffer at pH 7 by varying equilibrating time from 0 to 48 h. The isotherm studies were constructed from this data along with that from different concentration. The effect of the solution pH on the adsorption capacity was evaluated using 10 mM phosphate buffer at pH 5, 7 or 9. Furthermore, the effects of the HAN molecular structure on the selective adsorption at pH 7 was evaluated using individual and mixed solutes of the five different five HANs (MCAN, DCAN, TCAN, MBAN and DBAN), at the same concentration.

3. Results and discussion

3.1. Physicochemical characteristics of the synthesized adsorbents

The BET surface area and mean pore size (as diameter) were estimated and are summarized in Table 1. XRD patterns of the parental HMS and OD-HMS corresponded to the hexagonal porous structure, while A-HMS and M-HMS (functionalization via the co-condensation method) exhibited a decrease in the level of structure order (Fig. 1). The quantification of organosilanes revealed that the amine group content of A-HMS was equal to 9.037 $\mu mol_N\ m^{-2}$ and the sulfur content of M-HMS was 2.554 $\mu mol_S\ m^{-2}$ (Table 1).

Surface hydrophobic/hydrophilic characteristics reflect the water affinity of the adsorbents. In this study the hydrophobic surface adsorbents, M-HMS, OD-HMS and PAC, were analyzed for contact angle (θ). In general, the smaller the contact angle is, the greater the adsorbent surface exhibits hydrophilic characteristics. The contact angle attained from the M-HMS adsorbent was similar to that of the OD-HMS, but significantly larger than that for PAC (Table 1). Thus, PAC is more hydrophilic than either M-HMS or OD-HMS.

The surface charge density, as Cm^{-2}, of the parental HMS, the three functionalized HMS derivatives and PAC vs. the pH are plotted in Fig. 2. The pH_{PZC} of the parental HMS was 5.0 while two of the functionalized HMSs (A-HMS and M-HMS) exhibited a shift in

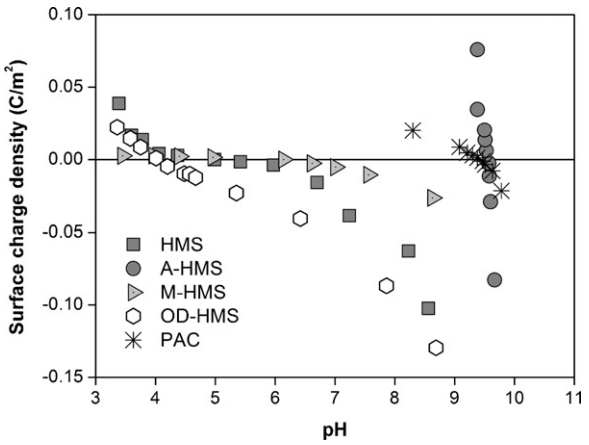

Fig. 2. Surface charge density of adsorbents as a function of the solution pH.

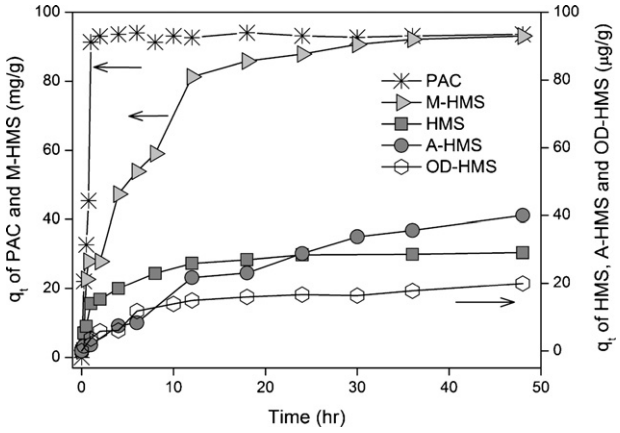

Fig. 3. DCAN adsorption kinetics of PAC and M-HMS at 50 mg L^{-1}, and HMS, A-HMS and OD-HMS at 100 μg L^{-1}.

the pH_{PZC} to 9.5 and 6.2, respectively, due to the presence of the amine- and mercapto-groups, respectively, which undergo protonation at low/moderate pH values. On the other hand, the OD-HMS was found to shift towards lower charged value (~4.0).

3.2. Adsorption kinetics

Kinetic curves for DCAN adsorption on the porous adsorbents are shown in Fig. 3. Note that the data for DCAN adsorption on PAC and M-HMS are plotted with a different *Y*-axis scale to the others due to the much higher (ca. 2300–4600-fold) adsorption capacities. A large amount of DCAN was adsorbed over PAC and M-HMS, but with PAC the equilibrium was reached within a short contact time (1 h) whereas with M-HMS it did not reach equilibrium but tended towards it at 36–48 h and was half maximal at ~5 h. In accordance, the acrylonitrile adsorption on PAC was reported to take about 1 h to attain equilibrium at an initial concentration of 100 mg L^{-1} [13]. For HMS and OD-HMS, the amount of adsorbed DCAN reached the equilibrium stage at approximately 18 h. Interestingly, the kinetic curves of M-HMS and A-HMS both showed a multi-step biphasic adsorption process. This is probably related to their low degree of pore order and wide pore size distribution.

Kinetic modeling, pseudo-first-order and pseudo-second-order models were employed to investigate the likely adsorption mechanism. The pseudo-first-order and pseudo-second-order equations can be represented as given in Eqs. (1) and (2):

$$q_t = q_e(1 - \exp^{-k_1 t}) \quad (1)$$

$$q_t = \frac{q_e^2 k_2 t}{1 + q_e k_2 t} \quad (2)$$

where q_t and q_e are the amount of DCAN adsorbed at any given time (t) and at equilibrium (mg g^{-1}), respectively. k_1 (h^{-1}) and k_2 (g mg^{-1} h^{-1}) are the rate constant for pseudo-first-order, and pseudo-second-order, respectively.

Based on the pseudo-second-order model, the initial adsorption rate, h (mg g^{-1} h^{-1}) at $t = 0$ can be estimated according to Eq. (3):

$$h = k_2 q_e^2 \quad (3)$$

In order to quantitatively compare the applicability of different kinetic models in fitting to the data, a normalized standard deviation Δq (%), was calculated as shown in Eq. (4):

$$\Delta q(\%) = 100 \times \sqrt{\frac{\sum [(q_{exp} - q_{cal})/q_{exp}]^2}{N - 1}} \quad (4)$$

where N is the number of data points, and q_{exp} and q_{cal} (mg g^{-1}) are the experimental and the calculated adsorption capacities, respectively. The best-fit models should have the least Δq (%) values.

The kinetic parameters, the correlation coefficients (R^2) and Δq (%) from the nonlinear equation, were calculated using the ORIGIN version 8.0 software and the results are shown in Table 2. Both models provided high and significant R^2 values, but these were not significantly different between the two models. However, the Δq (%) of the pseudo-second-order model was significantly smaller, regardless of the adsorbents, compared with those of the pseudo-first-order model. Thus, adsorption of DCAN onto these adsorbents is best represented with a pseudo-second-order kinetic model. Consistent with this notion is that Wu et al. [14] reported that the pseudo-second-order model was suitable to explain the adsorption of low molecular weight compounds on small adsorbent particles. Regardless, the initial adsorption rate (h) followed the order of PAC > M-HMS > HMS > OD-HMS > A-HMS.

The adsorption process over any porous adsorbent involves three consecutive mass transfer steps: (1) film or external diffusion, (2) pore diffusion and (3) adsorption at the site on the adsorbent surface [15]. The intraparticle diffusion model proposed by Weber and Morris [16] was adopted to verify the mechanism controlling

Table 2
Kinetic parameters of DCAN adsorption onto the indicated five adsorbents using the pseudo-first-order and pseudo-second-order kinetic models.

Adsorbents	$q_{e,exp}$ (μg g^{-1})	Pseudo-first-order				Pseudo-second-order				h (μg g^{-1} h^{-1})
		$q_{e,cal}$ (μg g^{-1})	k_1 (h^{-1})	R^2	Δq (%)	$q_{e,cal}$ (μg g^{-1})	k_2 (g μg $^{-1}$ h^{-1})	R^2	Δq (%)	
PAC[a]	94,060	94,025	1.2832	0.9835	1.782	98,604	19.270	0.9985	0.035	170,490
M-HMS[a]	95,030	91,311	0.1781	0.9595	2.900	102,430	2.4600	0.9723	0.162	22,210
HMS[b]	29.10	26.865	0.4516	0.9424	4.398	29.288	0.0213	0.9622	2.008	18.06
A-HMS[b]	73.45	75.787	0.0206	0.9884	0.815	75.827	0.0001	0.9891	0.451	0.67
OD-HMS[b]	18.94	17.532	0.1556	0.9702	1.677	20.681	0.0086	0.9729	0.202	3.09

[a] Initial DCAN concentration was 50 mg L^{-1}.
[b] Initial DCAN concentration was 100 μg L^{-1}.

Table 3
Kinetic parameters of DCAN adsorption onto the indicated adsorbents obtained using the intraparticle diffusion model.

Adsorbents	k_{iP1} ($\mu g\,g^{-1}\,h^{-0.5}$)	Intercept (C_1)	R^2	k_{iP2} ($\mu g\,g^{-1}\,h^{-0.5}$)	Intercept (C_2)	R^2
PAC	79,631	21,117	0.99	–	–	–
M-HMS	24,949	7,683.9	0.99	5,205	62,875	0.98
HMS	11.51	0.24	0.94	5.22	7.99	1.00
A-HMS	3.97	1.17	0.95	8.33	11.1	0.96
OD-HMS	14.29	0.58	0.99	1.82	18.0	0.98

the DCAN adsorption process, and can be defined as shown in Eq. (5):

$$q_t = k_{iP} t^{0.5} + C \quad (5)$$

where k_{iP} is the intraparticle diffusion rate constant ($mg\,g^{-1}\,h^{-0.5}$).

The data-fitting curves are shown in Fig. 4. Note that since the HMS and OD-HMS adsorbents showed very similar adsorption kinetics, only the fitting curve for HMS is presented for simplicity. The q_t vs. $t^{0.5}$ relations were found to display multi-linearity, indicating that multiple adsorption steps are involved in the adsorption process. Similar behaviors have been reported for the retention of various molecules on mesoporous silicates [17,18]. It can be seen that the adsorption over HMS (and OD-HMS, not shown) and M-HMS displayed three different regimes. The first regime represented the external mass transfer in the boundary layer while the second one was accounted for the diffusion of DCAN molecules through the pores of the adsorbent simultaneously with a gradual adsorption on the surface. Finally, the horizontal line at longer time points illustrated attaining the adsorption equilibrium. In the case of PAC, the external diffusion is not observed; the first linear regime can be reasonably correlated to the intraparticle diffusion. The adsorption of DCAN on A-HMS showed at least two phases but did not plateau out.

The rate constant of the first regime corresponds to the external mass transfer, where the larger the value the faster the external diffusion. The rate constant of these adsorbents are listed in Table 3, where it can be seen that the order of the rate constant was PAC > M-HMS ≫ OD-HMS > HMS > A-HMS. This is consistent with the level of hydrophobicity of the adsorbent surface, where the hydrophobic functional group might reduce the film resistance of water to mass transfer surrounding the adsorbent particle.

The intraparticle diffusion rate constant is determined from the slope of the second regime. The calculated values follow the sequence A-HMS > HMS > OD-HMS, and it implies that the pore size of the adsorbent might influence the adsorption rate. Due to the larger pore size of A-HMS, DCAN could diffuse into the pores more easily than the smaller pore size. However, the kinetic adsorption of DCAN on A-HMS did not reach the equilibrium plateau, which might be caused by the wide pore sizes distribution resulting from a disordered mesopore structure. Moreover, the existence of a boundary layer effect for HMS, A-HMS and M-HMS, as indicated by the fact that the linear plot does not pass through the origin, suggesting that intraparticle diffusion is not the only rate-limiting step for DCAN adsorption.

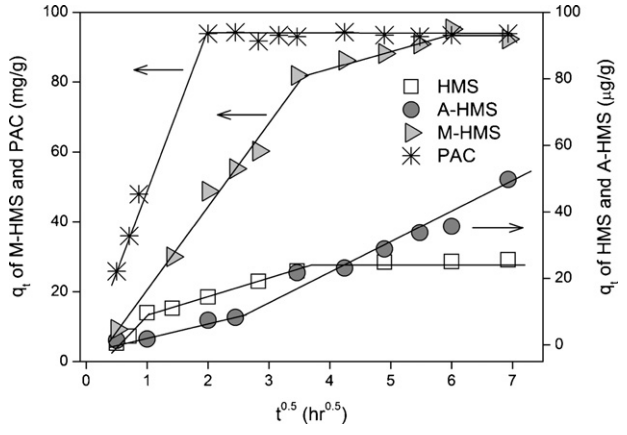

Fig. 4. Plot of intraparticle diffusion model (Weber and Morris) for the adsorption of DCAN on HMS, A-HMS, M-HMS and PAC.

3.3. Adsorption isotherms

Table 4 shows the calculated positive and negative charge distribution of the DCAN molecule after its structure was optimized for minimum energy using MOPAC. According to the molecular structure of DCAN, there are two possible reactive sites for the adsorption on the silica-based porous materials. The nitrogen atom (N3) of the nitrile group possesses some basicity and is prone to interact with electron-deficient sites, such as protons and Lewis acids. On the other end, the C≡N group and the two chloride atoms withdraw electrons from the methyl carbon (C2), leaving a positive charge on the hydrogen atom (H6). Besides the hydrophobic/hydrophilic characteristics of the adsorbent surface, two other important mechanisms, that is hydrogen bonding and electrostatic interaction (ion–dipole interaction), are proposed here to interpret the DCAN adsorption. Hydrogen bonding may occur via an interaction between the surface functional groups with –OH, –SH or $–NH_2$ moieties and the nitrogen atom of DCAN molecules. Furthermore, the surface functional groups ionizable under different pH conditions, for example ≡Si–O^-, ≡Si–R–S^- and ≡Si–R–NH_3^+ among others, can interact with the opposite charged positions of the DCAN molecules via electrostatic forces. Moreover, DCAN molecule can be both reversibly and irreversibly adsorbed on the M-HMS surface, which can be the result by interaction between the carbon (C1) of nitrile group and mercapto functional group [19].

FT-IR analysis was used in order to identify the presence of the hydrogen bonding interaction during the surface adsorption. HMS saturated with DCAN was prepared by equilibrating vacuum-dried mesoporous adsorbent in an organic solution of DCAN. Instead of water, *n*-hexane was used as the solvent to exclude any interference from the O–H stretching of physisorbed water molecules. As shown in Fig. 5, free silanol groups (≡Si–OH) on the virgin HMS

Table 4
Charge characteristics of the DCAN molecule.

Molecular structure of DCAN	Charges[a]	
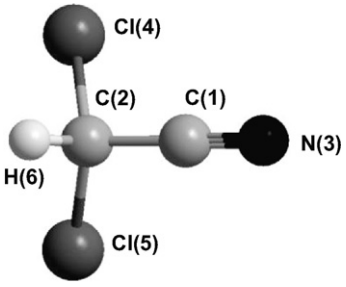	C (1)	−0.12548
	C (2)	−0.02396
	N (3)	−0.01778
	Cl (4)	−0.03625
	Cl (5)	−0.03648
	H (6)	+0.23995

[a] Calculated by ChemOffice Ultra 2005.

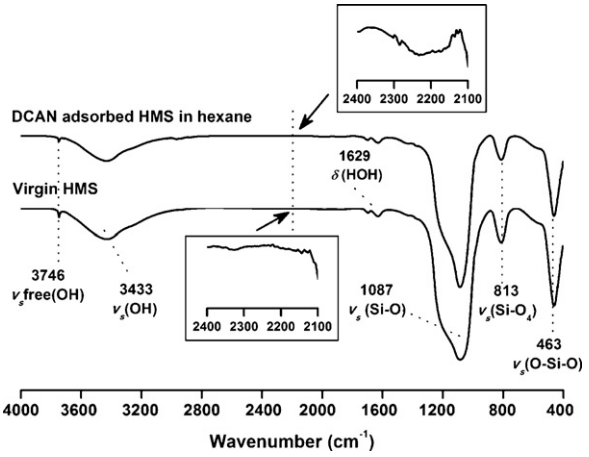

Fig. 5. Representative FT-IR spectra of virgin HMS and DCAN adsorbed HMS in hexane.

surface gave a sharp band at 3746 cm^{-1}. Upon adsorption of DCAN, a broad band from the C≡N stretching located at 2150–2300 cm^{-1} appeared [20] whereas the O–H stretching band remained intact. A downward shift concomitant with the broadening of the O–H stretching is evidence of hydrogen bonding between acetonitrile and the hydroxyl groups [20,21]. Therefore, it can be concluded that hydrogen bonding was not likely to be the major mechanism for the DCAN adsorption under the conditions investigated since the surface silanol must be clouded with water molecules and is not free for any significant interaction with DCAN in a real aqueous solution.

Comparison on the effects of the different surface functional groups of the HMS derivatives on the DCAN adsorption capacities is shown in Fig. 6a. M-HMS adsorbed the DCAN molecules far more effectively than HMS and the other two functionalized-HMS derivatives. As revealed in Fig. 2, the surface of M-HMS exhibited a moderately negative charge at pH 7. Consequently, the mercapto-groups as well as the remaining silanol groups were ionized and so the DCAN molecules were electrostatically adsorbed. Moreover, this result suggested that the hydrophobic surface (M-HMS; see below for OD-HMS) facilitated a higher adsorption capacity than the hydrophilic one (HMS and A-HMS) by probably reducing the competitive adsorption between water and DCAN onto the adsorbents. Recently, Punyapalakul et al. [7] pointed out that both electrostatic and hydrogen bonding interactions were interfered with by the presence of water especially at low concentrations of the adsorbate. In contrast, the hydrophobic OD-HMS adsorbent showed a lower adsorption performance even though its surface hydrophobicity was similar to M-HMS, as reflected by the contact angle (θ) (Table 1). Hence, the much higher DCAN adsorption capacity of M-HMS should be ascribed to the combination of its hydrophobic surface and ionizable mercapto-groups promoting the ion–dipole interaction, whereas the protonation/deprotonation of the octyl groups on OD-HMS surface cannot occur.

With respect to HMS, its negative surface charge could contribute to ion–dipole electrostatic interactions towards DCAN adsorption at pH 7. However, that the observed adsorption capacity of HMS for DCAN was lower than that for M-HMS might be caused by active surface competition between DCAN and water molecules. Along these lines, Pan and Jaroniec [22] reported that water molecules can be adsorbed onto the surface oxygen groups by hydrogen bonding. In our case study, the hydrophobic mercapto-groups can weaken the competition of water in aqueous solution and so result in the adsorption of DCAN.

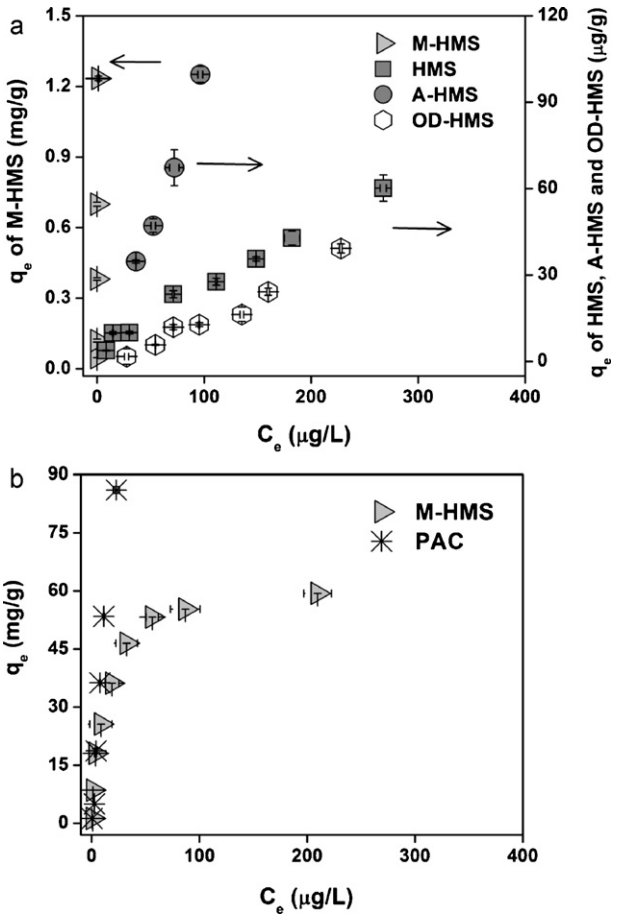

Fig. 6. DCAN adsorption capacities of HMS, the three functionalized HMS derivatives and PAC, showing (a) HMS and the three functionalized derivatives, (b) PAC and M-HMS.

A-HMS presents a positive charge surface over the pH range used in this study due to protonation of the amino group. Since DCAN contains a N-atom with one pair of electrons and a high electronegativity (negative dipole), DCAN can be electrostatically adsorbed onto the positively charge surface. Thus, A-HMS had a much higher DCAN adsorption capacity than the parental HMS and the functionalized OD-HMS derivative. To exclude the effect of surface area, at equilibrium concentration of 100 $\mu g\,L^{-1}$, the order of adsorption capacity per unit surface area were ranked as A-HMS > HMS ≅ OD-HMS (0.380, 0.033 and 0.032 $\mu g\,m^{-2}$, respectively). These results strongly support the effects of the surface functional group of HMS derivatives on DCAN adsorption.

The considerably higher adsorption capacity of PAC for DCAN was probably caused by its heterogeneous surface that consists of various organic functional groups [13,23]. Interestingly, M-HMS was only the functionalized silica-based material that had a comparable adsorption capacity to PAC for DCAN (Fig. 6b). Moreover, comparing between two silanol group-based adsorbents which have different surface area, i.e. HMS (712 $m^2\,g^{-1}$) and SBA-15 (654 $m^2\,g^{-1}$), exhibits similar adsorption capacities per unit surface area (0.0330 and 0.0335 $\mu g\,m^{-2}$ for HMS and SBA-15, respectively) (data not shown). Hence, it can be indicated that increasing of specific surface area of adsorbents can enhance DCAN adsorption capacities.

3.3.1. Isotherm models

In order to model the adsorption mechanism, Langmuir, Freundlich and Sips isotherm models were used to test the experimentally derived adsorption process data for correlation. The

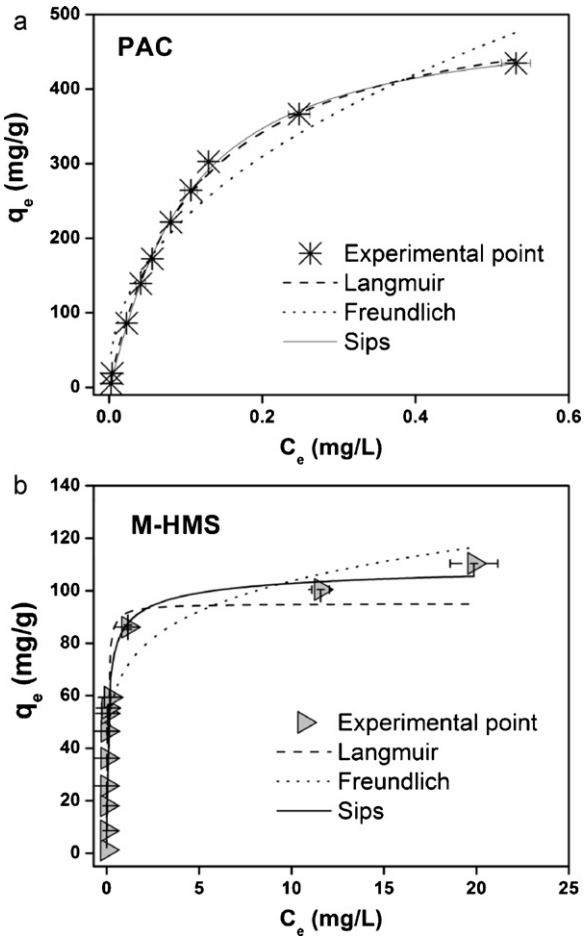

Fig. 7. Comparison of the predicted and experimental data for the equilibrium adsorption of DCAN on (a) PAC and (b) M-HMS adsorbents.

Langmuir and Freundlich equations can be defined as shown in Eqs. (6) and (7):

$$q_e = \frac{q_m K_L C_e}{1 + K_L C_e} \quad (6)$$

$$q_e = K_F C_e^{1/n} \quad (7)$$

where q_m is the maximum adsorption capacity (mg g^{-1}), K_L is Langmuir constant, and K_F and n are Freundlich constants.

The Sips model is used as a compromise between the Langmuir and Freundlich models, and can be written as in Eq. (8):

$$q_e = \frac{q_m K_S C_e^{1/n}}{1 + K_S C_e^{1/n}} \quad (8)$$

where K_S is the Sips adsorption constant.

In this work, the adsorption isotherm of PAC and M-HMS showed a L-shaped and H-shaped response, respectively, as shown in Fig. 7(a) and (b). The adsorption capacity results were fitted with the three models by nonlinear regression, while the other adsorbents (HMS, A-HMS and OD-HMS) were fitted with the linear isotherm due to the fact they showed a linear-shaped adsorption plot at a low initial concentration of DCAN. The linear model can be written as Eq. (9):

$$q_e = K_p C_e \quad (9)$$

where K_p is linear partition coefficient that obtained from the slope of plotted q_e vs. C_e.

The isotherm parameters of DCAN adsorption on M-HMS and PAC are listed in Table 5. As with Fig. 7, the Sips model showed the best fitting for both PAC and M-HMS (Table 5), supported by the R^2 and Δq (%) values for the three isotherms. That the Sips model is the best fit is reasonable due to its incorporation of the advantages of both the Langmuir and Freundlich equations, which can be applied either to homogeneous or heterogeneous surfaces. In this study, the exponent $1/n$ value for PAC was fairly close to unity, which means that the form of the DCAN adsorption equilibrium on PAC was more Langmuir like than Freundlich. Thus, the adsorption is limited with monolayer coverage and the surface is relatively homogeneous. A similar model has been observed previously for adsorption of another nitrile adsorbate (acrylonitrile) by PAC and GAC [13]. In contrast, M-HMS tends towards a Freundlich isotherm with the value of exponent $1/n$ being less than half and near zero in the Sips and Freundlich models, respectively, and suggests that the adsorption process on M-HMS is heterogeneous. In addition, a linear isotherm could be fitted to the results for HMS, A-HMS and OD-HMS with high R^2 values (>0.94). A high K_p value indicates a high affinity, and the observed order of the K_p constant was A-HMS > HMS > OD-HMS (Table 5).

Table 5
Isotherm parameters of DCAN adsorption on PAC and various HMS-based adsorbents.

Isotherms	PAC	M-HMS
Langmuir		
q_m (mg g^{-1})	531.78	92.613
K_L (L mg^{-1})	9.0024	38.606
R^2	0.9972	0.8521
Δq (%)	1.7693	12.945
Freundlich		
$1/n$	0.4409	0.1601
K_F (mg g^{-1})	629.26	71.023
R^2	0.9394	0.9092
Δq (%)	1.1462	2.2850
Sips		
q_m (mg g^{-1})	495.33	119.76
q_m per surface area (mg m^{-2})	0.5054	0.1313
Density of mercapto group (molecule m^{-2})	–	1.54E+18
Molar ratio (DCAN: mercapto)	–	0.4675
K_S (L mg^{-1})	14.565	2.3420
$1/n$	0.8354	0.4164
R^2	0.9984	0.9665
Δq (%)	1.8372	1.6411

Linear	HMS	A-HMS	OD-HMS
K_p	0.2370	0.9930	0.1540
R^2	0.9581	0.9784	0.9411

3.4. Effect of pH on DCAN adsorption

The adsorption capacity of DCAN on the different adsorbents within the pH range of 5–9 was evaluated, with the results presented in Fig. 8. Increasing the pH resulted in a higher DCAN adsorption on all five adsorbents (PAC, HMS, A-HMS, M-HMS and OD-HMS). The surface of the HMS, A-HMS and OD-HMS adsorbents is more negatively charged at pH 9, which is at a pH higher than their pH_{PZC}. The charge of the H-atom in the DCAN molecule, as calculated by ChemOffice Ultra 2005, is more positive (Table 4), and so the negative surface charges of these adsorbents could be electrostatically attracted by the positive dipole of the H-atom in DCAN molecules via ion–dipole electrostatic interaction. In addition, the density of the negative surface charge (per square meter) at pH 9 of the adsorbents was higher than that at pH 5 and 7, leading to a higher adsorption capacity. For A-HMS, surface of A-HMS is positively charged at pH 5–9 based on pH_{PZC} value (Table 1), however, at pH 9 the ratio of negative/positive charged moieties of A-HMS surface becomes higher than pH 5 and 7. This can increase the opportunity of negative groups on

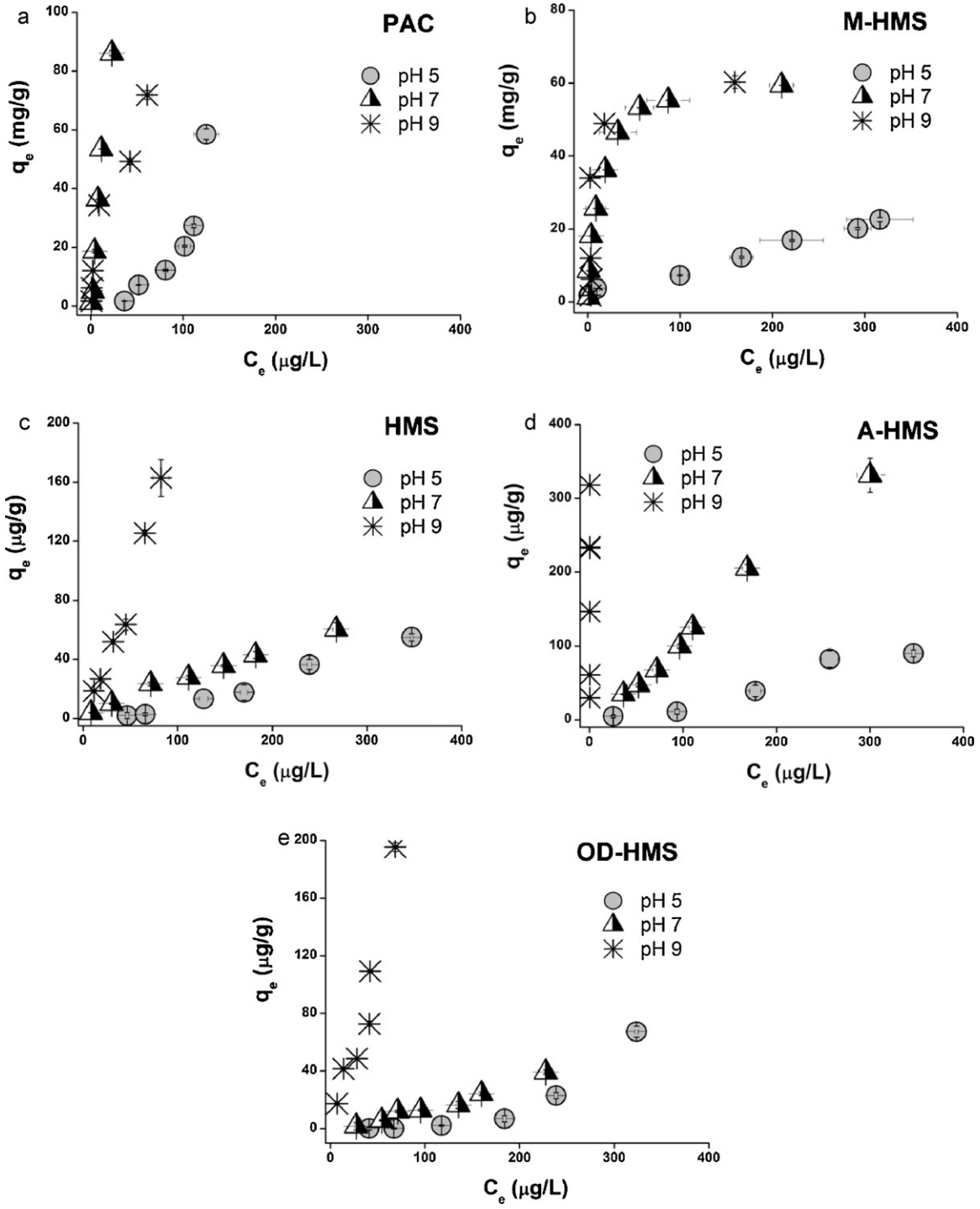

Fig. 8. Effect of pH on the adsorption of DCAN onto (a) PAC, (b) M-HMS, (c) HMS, (d) A-HMS and (e) OD-HMS in 10 mM phosphate buffer pH 5, 7 and 9.

surface to interact with the positive dipole of H-atom in DCAN molecule.

However, that the adsorption capacity of M-HMS was not significantly affected by increasing the pH from 7 to 9, accords with the fact that the surface charge density of M-HMS did not change significantly within the pH range 7–10 (Fig. 2). For PAC, the observed adsorption capacity at pH 7 was slightly higher than at pH 9, both the effect of pH on the complex surface functional groups of PAC and its interaction with DCAN to alter the adsorption capacity is still unclear.

3.5. Selective adsorption of HANs in single-solute and mixed-solute solutions

The individual adsorption isotherms for the five different HAN adsorbates by M-HMS were ranked in the adsorption preference order of TCAN ≅ DBAN > DCAN > MBAN > MCAN on M-HMS (Fig. 9a). Tri- and di-HANs, which had a high molecular weight, exhibited higher adsorption capacities on M-HMS compared with the mono-HANs. That the bromo-HANs had higher adsorption capacities than the chloro-HANs is due to the stronger positive dipole of the H-atom

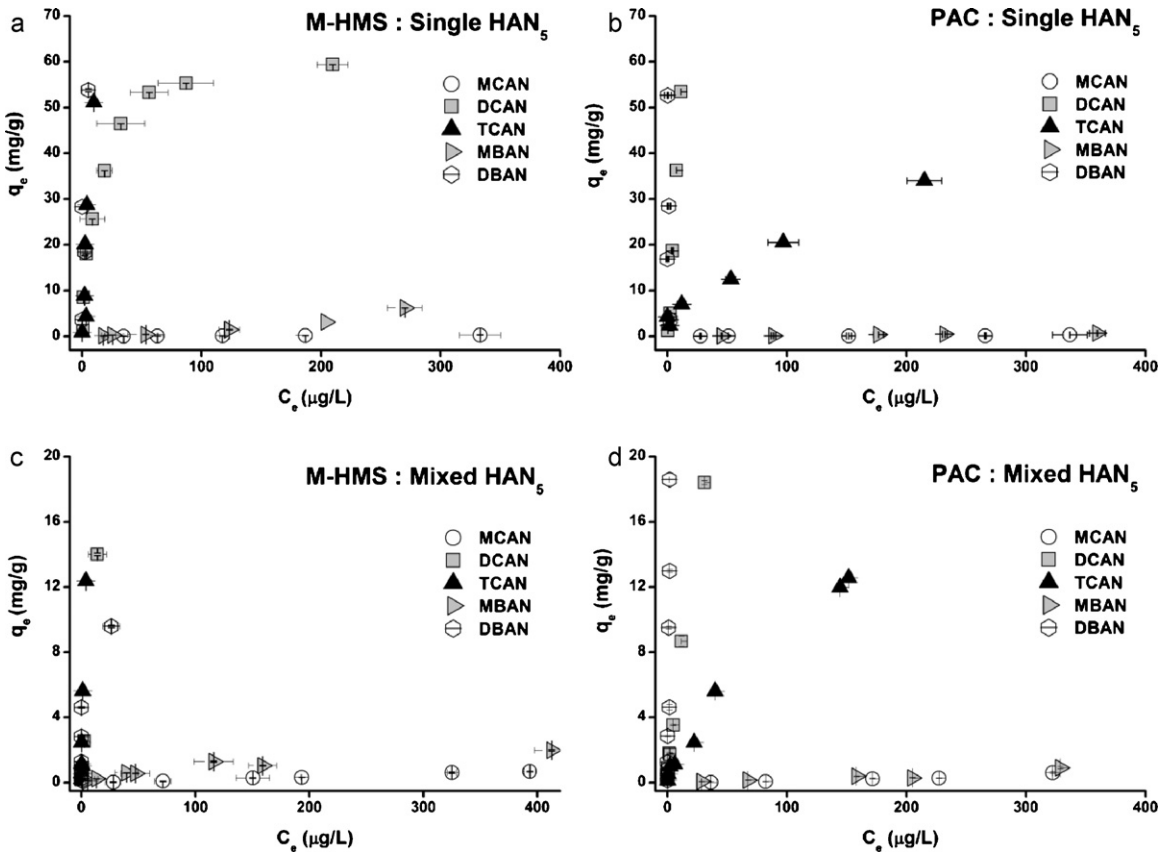

Fig. 9. Adsorption isotherm of the five HAN compounds as a (a, b) single solute and (c, d) mixed solute on the adsorbents in 10 mM phosphate buffer pH 7.

in bromo-HANs. These results indicate that the adsorption capacity of the five different HANs on M-HMS are likely to be related to the molecular structure of each HAN, though this requires further research for confirmation. In contrast, PAC had the highest adsorption capacities for di-HANs followed by tri- and mono-HANs, respectively (Fig. 9b). The individual adsorption capacities of the five HAN adsorbates on PAC then, in contrast, did not appear to directly relate to the types and amount of halogen atom in the molecule (Fig. 9b).

The adsorption isotherms of the mixed solutes of all five HANs together are shown in Fig. 9(c) and (d) for M-HMS and PAC, respectively. It was clear that the active surfaces of PAC and M-HMS were competitively segregated for all five HAN species in the mixed solute, causing a decreased adsorption capacity for each HAN. The order of adsorption capacities in the mixed solute on M-HMS was slightly different from the single solute results, being TCAN ≅ DCAN > DBAN > MBAN > MCAN. Thus, the DBAN adsorption capacity on M-HMS might be easily outcompeted and interrupted by the presence of the other HANs. However, on PAC the order of adsorption capacities of all HANs was in the same as that seen with the single solute (Fig. 9d).

4. Conclusions

DCAN adsorption on all five tested adsorbents followed a pseudo-second order rate kinetics model. The adsorption process was dependent on both the boundary layer effect and the intraparticle diffusion. The Sips isotherm model was successfully applied to describe the adsorption mechanism on PAC and M-HMS. The surface functional groups significantly affected the DCAN adsorption capacity, since this adsorptive interaction involves electrostatic interactions related to the pH_{PZC} of adsorbents. Interference by water molecules at low concentrations of DCAN strongly affected the adsorption mechanism. In addition, DCAN adsorption is highly pH dependent, being favored at a high pH due to having a higher negative surface charge density. The molecular structure of the five HANs did not affect the adsorption capacities and selectivity on PAC, while they strongly affected those of the 3-mercaptopropyl-grafted HMS.

Acknowledgements

The authors are grateful for the financial support from the 90th anniversary of Chulalongkorn University Fund (Ratchadaphiseksomphot Endowment Fund), Center of Excellence for Environmental and Hazardous Waste Management (EHWM) of Chulalongkorn University, Funding from "Fate and Removal of Emerging Micropollutants in Environment" project under Special Task Force for Activating Research (STAR) of Chulalongkorn University, 2010 TTSF Science & Technology Research Grant from Thailand Toray Science Foundation and 2010 Overseas Research Grants from the Asahi Glass Foundation. The technical support from Department of Environmental Engineering, Faculty of Engineering and the Center for Petroleum, Petrochemicals and Advanced Materials, Chulalongkorn University are also acknowledged.

References

[1] H.-H. Tung, R.F. Unz, Y.F. Xie, HAA removal by GAC adsorption, J. Am. Water Works Assoc. 98 (2006) 107–112.
[2] C. Ratasuk, C. Kositanont, C. Ratanatamskul, Removal of haloacetic acids by ozone and biologically active carbon, J. Sci. Soc. Thai. 34 (2008) 293–298.
[3] J. Kim, B. Kang, DBPs removal in GAC filter-adsorber, Water Res. 42 (2008) 145–152.

[4] K.G. Babi, K.M. Koumenides, A.D. Nikolaou, C.A. Makri, F.K. Tzoumerkas, T.D. Lekkas, Pilot study of the removal of THMs, HAAs and DOC from drinking water by GAC adsorption, Desalination 210 (2007) 215–224.
[5] V. Uyak, I. Koyuncu, I. Oktem, M. Cakmakci, I. Toroz, Removal of trihalomethanes from drinking water by nanofiltration membranes, J. Hazard. Mater. 152 (2008) 789–794.
[6] P. Punyapalakul, S. Takizawa, Effect of organic grafting modification of hexagonal mesoporous silicate on haloacetic acid removal, Environ. Eng. Res. 41 (2004) 247–256.
[7] P. Punyapalakul, S. Soonglerdsongpha, C. Kanlayaprasit, C. Ngamcharussrivichai, S. Khaodhiar, Effects of crystalline structures and surface functional groups on the adsorption of haloacetic acids by inorganic materials, J. Hazard. Mater. 171 (2009) 491–499.
[8] B. Lee, Y. Kim, H. Lee, J. Yi, Synthesis of functionalized porous silicas via templating method as heavy metal ion adsorbents: the introduction of surface hydrophilicity onto the surface of adsorbents, Micropor. Mesopor. Mater. 50 (2001) 77–90.
[9] K. Inumaru, T. Nakano, S. Yamanaka, Molecular selective adsorption of alkylphenols and alkylanilines from water by alkyl-grafted mesoporous alumina: a comparative study to alkyl-grafted mesoporous silica, Micropor. Mesopor. Mater. 95 (2006) 279–285.
[10] P. Punyapalakul, S. Takizawa, Selective adsorption of nonionic surfactant on hexagonal mesoporous silicates (HMSs) in the presence of ionic dyes, Water Res. 40 (2006) 3177–3184.
[11] M.M. Smart, R.G. Rada, G.N. Donnermeyer, Determination of total nitrogen in sediments and plants using persulfate digestion. An evaluation and comparison with the Kjeldahl procedure, Water Res. 17 (1983) 1207–1211.
[12] EPA Method 551.1, Determination of Chlorination Disinfection Byproducts, Chlorinated Solvents and Halogenated Pesticides/Herbicides in Drinking Water by Liquid–Liquid Extraction and Gas Chloromatography with Electron-capture Detection, National Exposure Research Laboratory, Office of Research and Development, U.S. Environmental Protection Agency, Cincinnati, OH, 1990.
[13] A. Kumar, B. Prasad, I.M. Mishra, Adsorptive removal of acrylonitrile by commercial grade activated carbon: kinetics, equilibrium and thermodynamics, J. Hazard. Mater. 152 (2008) 589–600.
[14] F.-C. Wu, R.-L. Tseng, S.-C. Huang, R.-S. Juang, Characteristics of pseudo-second-order kinetic model for liquid-phase adsorption: a mini-review, Chem. Eng. J. 151 (2009) 1–9.
[15] Q.-S. Liu, T. Zheng, P. Wang, J.-P. Jiang, N. Li, Adsorption isotherm, kinetic and mechanism studies of some substituted phenols on activated carbon fibers, Chem. Eng. J. 157 (2010) 348–356.
[16] W.J. Weber, J.C. Morris, Kinetics of adsorption on carbon from solution, J. Sani. Eng. Div. ASCE 89 (1963) 561–578.
[17] Q. Qin, J. Ma, K. Liu, Adsorption of anionic dyes on ammonium-functionalized MCM-41, J. Hazard. Mater. 162 (2009) 133–139.
[18] J. Li, L. Wang, T. Qi, Y. Zhou, C. Liu, J. Chu, Y. Zhang, Different N-containing functional groups modified mesoporous adsorbents for Cr(VI) sequestration: Synthesis, characterization and comparison, Micropor. Mesopor. Mater. 110 (2008) 442–450.
[19] S. Patai, The Chemistry of the Thiol Group: Part 2, John Wiley and Sons, London, 1974.
[20] G. Busca, T. Montanari, M. Bevilacqua, E. Finocchio, Removal and recovery of nitriles from gaseous streams: an IR study of acetonitrile adsorption on and desorption from inorganic solids, Colloids Surf. A: Physicochem. Eng. Aspects 320 (2008) 205–212.
[21] P. Kozyra, I. Salla, T. Montanari, J. Datka, P. Salagre, G. Busca, FT-IR study of the adsorption of carbon monoxide and of some nitriles on Na-faujasites: additional insight on the formation of complex interactions, Catal. Today 114 (2006) 188–196.
[22] D. Pan, M. Jaroniec, Adsorption and thermogravimetric studies of unmodified and oxidized active carbons, Langmuir 12 (1996) 3657–3665.
[23] J.-H. Tsai, H.-M. Chiang, G.-Y. Huang, H.-L. Chiang, Adsorption characteristics of acetone, chloroform and acetonitrile on sludge-derived adsorbent, commercial granular activated carbon and activated carbon fibers, J. Hazard. Mater. 154 (2008) 1183–1191.